

Optical properties of porous Si/PECVD SiN_x:H reflector on single crystalline Si for solar cells

L. REMACHE^{1*}, T. NYCHPORUK², N. GUERMIT¹, E. FOURMOND², A. MAHDJOUR¹, M. LEMITI²

¹Laboratoire des Matériaux et Structure des Systèmes Electromécaniques et leur Fiabilité,
LMSSEF Université Larbi Ben Mhidi, Algérie

²Institut des nanotechnologies de Lyon, INL, CNRS-UMR5270, INSA, Villeurbanne F-69621, France

The improvement of optical confinement on the back crystalline silicon solar cell is one of the factors leading to its better performance. Porous silicon (PS) layer can be used as a back reflector (BR) in solar cells. In this work, single layers of porous silicon were grown by electrodeposition on a single crystalline silicon substrate. The measurement of the total reflectivity (R_T) on Si/PS surface showed a significant improvement in optical confinement compared to that measured on Si/standard Al back surface field (BSF). The internal reflectivity (R_B) extracted from total reflectivity measurements achieved 86 % for the optimized single PS layer (92 nm thick layer with 60 % porosity) in the wavelength range between 950 and 1200 nm. This improvement was estimated as more than 17 % compared to that measured on the surface of Si/BSF Al contact. To improve the stability and passivation properties of PS layer BR, silicon nitride layer (SiN_x) was deposited by PECVD on a PS layer. The maximum measured total reflectivity for PS/SiN_x achieved approximately 56 % corresponding to an improved R_B of up to 83 %. The PS formation process in combination with the PECVD SiN_x, can be applied in the photovoltaic cell technology and offer a promising technique to produce high-efficiency and low-cost c-Si solar cells.

Keywords: *porous silicon; light trapping; SiN_x; total reflectivity; internal reflectivity*

© Wrocław University of Technology.

1. Introduction

Currently, most of the industrially produced solar cells are based on the use of silicon. Hence, reducing the amount of silicon, by thinning the wafer is a key point in limiting the overall photovoltaic cell cost, making the price of energy from solar cells competitive with the conventional systems [1–4]. However, when using very thin solar cell (less than 150 μm), it is necessary to optimize carefully the internal reflection on the backside of the cell.

The objective is to achieve a reasonable efficiency that makes such cells cost-effective compared to conventional crystalline silicon substrate. Most of the PV industry still uses the classical process based on Al BSF with all the technology limitations and problems it implies [4, 5]. Indeed, this leads to poor performance in surface recombination velocity, moderate optical confinement and

mechanical stress in the wafer during high temperature processes [5, 6]. This recent change therefore forces the industry to adopt new technologies which are reliable and compatible with cost effective industrial processes. However, light trapping within the cell is necessary to obtain the light absorption in the range of 800 to 1200 nm [4, 7]. Therefore, to replace the classical Al BSF, an effective back reflector structure needs to be developed and implanted successfully into the cell [5–8].

The study of optical confinement in the rear contact silicon solar cell can be performed on p-type crystalline silicon substrate, without considering the effect of the emitter (n+) and the antireflection coating on the front surface of the cell, which also take part in light transmission and reflection.

In this context, some groups developed new photovoltaic structures to improve the optical confinement within the cell. Nitride and silicon oxide deposited by PECVD are used in two possible variants: SiN/SiO, SiO/SiN/SiO [5, 8, 9]. These

*E-mail: rlouardi@yahoo.fr

dielectric structures provide good passivation on the front and the rear surface of a solar cell [9–12]. However, they do not effectively contribute to the increase of the optical confinement [5]. Distributed Bragg reflector is a structure composed of a multilayer stack of high and low refractive index layers. Several configurations were published: Bragg mirrors implemented with (i) amorphous silicon and silicon oxide [1], (ii) SiN_x and SiO_x dielectric [12] (iii) porous silicon of two alternating porosities [2, 7, 13–15]. The design of porous silicon Bragg mirror is complex and requires appropriate control of optical parameters of its constituent layers, and it produces many losses at the interface due to the excessive stack of porous silicon layers [3, 16].

However, the advantage of the porous silicon used as a backside reflector for a solar cell, is the possibility for implementing on its surface both types of back metal contact (full and local Al BSF) [17–19].

In this work, we concentrated on studying rear structures containing single porous silicon layers and PS/SiN_x:H (SiN) with a fixed stoichiometry to investigate their light trapping behaviors without capping Al.

The PS layers were elaborated by electrochemical anodization, and SiN_x dielectric layers were deposited using low frequency plasma enhanced chemical vapor deposition (PECVD) at moderated temperature (370 °C) with ammonia (NH₃) and silane (SiH₄) as precursor gases.

2. Experimental

The experiments were carried out on CZ (1 0 0) p-type silicon substrates with a resistivity of 0.01 to 0.02 Ω·cm and a thickness of 250 to 300 μm. Alternatively, surface doping of standard solar cell wafers of 1 to 10 Ω·cm could be used for the same purpose. Porous silicon (PS) was grown on the front polished side in a mixture containing HF (48 %) and C₂H₅OH (volumetric ratio equal to 1). The electrochemical cell was made from Teflon and had a circular aperture with a diameter of 1.5 cm, on which the silicon wafer was sealed.

A platinum wire was used as a cathode at a distance of 2 cm from the Si wafer surface, which acted as the anode. The process was carried out at room temperature.

After etching, all samples were rinsed in ethanol and dried in air. To obtain the adequate refractive index for the PS, the current density was fixed at 100 mA/cm², and the thickness of the layer was controlled by the anodization time.

SiN_x:H films were deposited using pure silane and ammonia (SiH₄, NH₃) as precursors gases in a vertical semi-industrial, low frequency (440 kHz) PECVD reactor (LF-PECVD) from SEMCO Engineering (described in the literature [20, 21]). The deposition was made at 370 °C, with a power density of 0.26 W/cm², a pressure of 200 Pa, and a NH₃/SiH₄ gas flow ratio equal to 5. The deposition rate was 29 nm/s.

Horiba-Jobin Yvon Uvisel Spectroscopic Ellipsometer (SE) in conjunction with the Bruggemann effective medium approximation (EMA) and the Tauc-Lorenz model were used to determine the optical parameters of the prepared structures (refractive indexes and thicknesses) in the range of 1.5 to 5 eV [21, 22]. Structural properties of the prepared samples were characterized by scanning electron microscopy (SEM) using a MIRA3 TESCAN. The total reflectance on the front surface was measured within the 300 to 1200 nm wavelength range by an optical reflectometer that included an integrating sphere. An optical analysis to extract the internal rear reflectivity is presented in Section 3.3.

3. Results and discussion

3.1. Porous silicon layer

The PS layer was optimized using a quarter-wavelength criterion to maximize the total reflectivity on the front surface of the Si/PS structure:

$$nd = \lambda/4 \quad (1)$$

where n is the refractive index and d is the thickness of the layer which should have a maximum reflectance at the wavelength λ_0 (around 700 nm) where the highest photon density occurs.

The refractive index of the back reflector (BR) was calculated by using transfer matrix method and Bruggeman effective medium approximation (EMA), detailed in the literature [23–25] which allowed us to combine the polycrystalline silicon (pc-Si) and void [26]. For silicon substrate, we used refractive indexes published by Palik [27].

Indeed, a porosity of 80 % of the silicon leads to a refractive index below 1.47 (at $\lambda_0 = 700$ nm). This entails an important rise of refractive index compared to silicon substrate (3.78), which can lead to an increase in the reflectivity greater than 70 %. However, the stability of the porous layer requires a porosity value not exceeding 65 % that corresponds to a refractive index of 1.93 [28–30]. In that case, the calculation resulted in a designed thickness of approximately 92 nm for a refractive index equal to 1.90, corresponding to a porosity of 60 %. In order to obtain the porosity of the PS layer around 60 %, the current density was fixed at 100 mA/cm^2 [31]. The thickness of the layer was controlled by anodization time. It is also interesting to measure the average growth kinetics of a porous silicon grown on P^+ substrate. The thickness of the PS layer increases almost linearly with the etching time when every other etching parameter is kept fixed (Fig. 1). We can also notice that the average growth kinetics is around 85.7 nm/s in the employed range of anodization time.

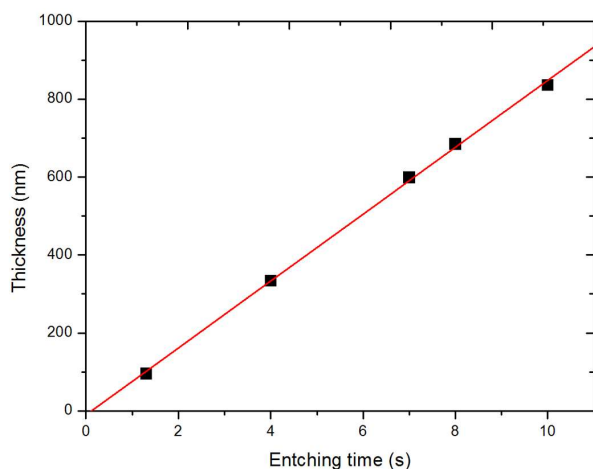


Fig. 1. Thickness vs. etching time of PS grown at a constant current density of $100 \text{ mA}\cdot\text{cm}^{-2}$ on a polished p^+ substrate.

The optimum thickness for the PS (BR) was obtained by varying the anodization time in the range of 1.3 to 10 s; the weighted average value for the measured total reflectivity was calculated in the range of 800 to 1200 nm (Table 1). The values of the thickness for each layer were determined from the spectroscopic ellipsometry (SE) measurements and SEM images. The results show that the maximum reflectivity is equal to 55 % for the thickness of 96 nm and 79 nm obtained using the (SE) measurement and (SEM) image, respectively, which corresponds to 1.3 s of anodization. This value can be the most appropriate to achieve the optimal thickness for the BR based on a single PS layer.

Table 1. Weighted average reflectivity calculated from the measured total reflectivity in the wavelength range between 800 and 1200 nm, for various thicknesses of PS layers.

	Weighted average R [%]	Thickness [nm] SE	Thickness [nm] SEM
1.3	52	96	79
4	50	334	329
7	48	599	560
8	47	685	660
10	44	836	836

Structural morphology (planar and cross-sectional views) was examined by SEM. Fig. 2 shows the surface morphology of the structure in SEM planar view. The array of void spaces (dark) in the silicon matrix (bright) can be seen clearly in the planar view SEM image. The morphology of the structure shows that the electrochemical etching has been uniform on the surface and created the granular structures of spherical shapes. A large number of pores distributed in all directions with a mean pore size of 8 to 15 nm can be observed in Fig. 2. On the other hand, the cross-section SEM image shows good agreement with the SE results. Indeed, the thickness is of ~ 79 nm, and it is perfectly uniform indicating that the rapid etching process forms a uniformly porous layer.

The wavelength dependence of the total reflectivity of the PS grown on the silicon substrate

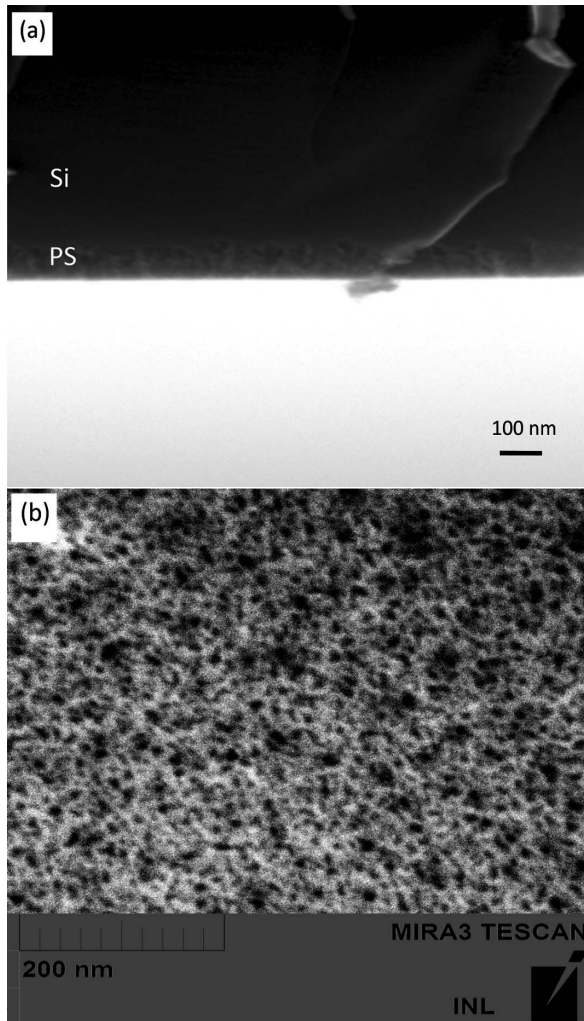


Fig. 2. Cross-section SEM image of Si/PS structure obtained during 1.3 s at current density of 100 mA/cm² on p⁺ substrate (a), planar view of the fabricated porous silicon layer (b).

at a current density of 100 mA/cm² and an etching time of 1.3 s is depicted in Fig. 3. The spectroscopic ellipsometry measurement revealed that the optimum thickness was around 96 nm whereas the optimum porosity was equal to 62.3 %. A certain effect of a light confinement effect brought by the single PS layer, which was observed in the wavelength range between 600 and 950 nm, led to a significant increase in reflectance ($R_T \sim 4\%$) in this wavelength region, while in the infrared region the increase of total reflectivity was clearly observed. Besides, maximum measured reflectivity in the range

between 950 and 1200 nm achieved 58.5 % for the optimized parameters of a single PS layer. This improvement was estimated as more than 12 % compared to that measured on the surface of Si/BSF Al contact.

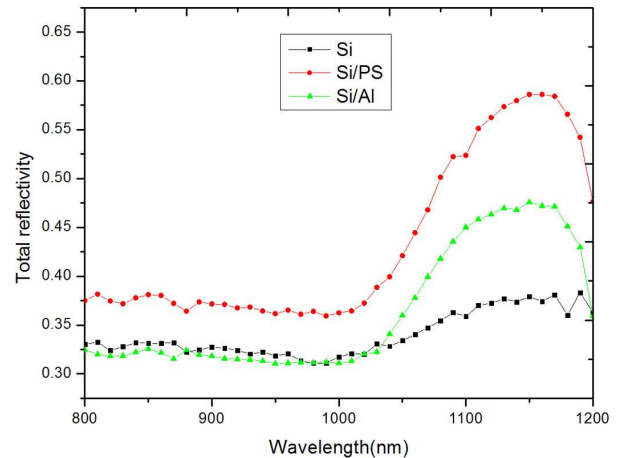


Fig. 3. Experimental total reflectivity spectra for Si/PS and Si/Al.

3.2. PS/SiN_x layers

It was shown in the previous section that the porous silicon can contribute to the improvement of optical confinement in the back side of solar cell. However, the surface recombination velocity strongly increases when using PS layers, due to the roughness of the surface [20]. The optical properties of PS layers may also degrade in time when no further treatment is used. The deposition of a silicon nitride (SiN_x:H) layer over the PS layer may be an alternative solution. Indeed, we have demonstrated experimentally in the previous paper [32], that the silicon nitride layer deposited over the PS layer on the front surface of a solar cell improved the passivation properties by more than 20 %.

On the other hand, the silicon nitride deposited in the LF-PECVD reactor is transparent in the range of 800 to 1200 nm and exhibits a wide range of refractive indexes (between 1.84 and 3 at 633 nm). To optimize the parameters of the PS/SiN_x bilayer, the dielectric layer must be designed to maximize the total reflectivity.

The thicknesses of the layers were calculated by using the following formula:

$$n_{PS}d_{PS} = n_{SiN_x}d_{SiN_x} = \lambda/4 \quad (2)$$

where n_{PS} and d_{PS} are the thickness and the refractive index for the PS layer calculated in section (3.1).

The refractive index for the SiN_x layer is equal to 2.4 at 700 nm ($R = NH_3/SiH_4 = 5$), the calculated thickness is equal to 73 nm.

Fig. 4 shows the cross-section SEM images of PS/ SiN_x structures deposited on silicon substrate. This image shows that the thickness is uniform throughout the deposited SiN_x and indicates that the deposition process of the porous layer (grown during 1.30 s), was successfully carried out on the rough PS surface. This can be confirmed by the morphology of the PS surface shown in the SEM image in Fig. 2b. The mean pore size less than 15 nm facilitated the deposition of the dielectric layer, and avoided its diffusion into the PS layer. On the other hand, the conditions of PECVD deposition did not affect the thickness of the porous layer. Besides, it can be seen that the thickness of the SiN_x layer is of ~ 75 nm.

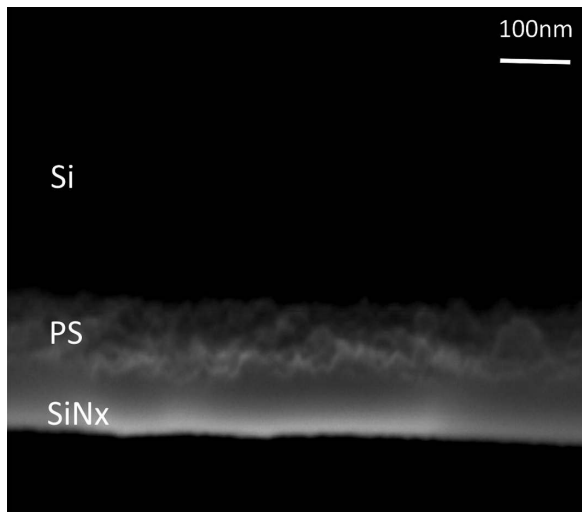


Fig. 4. Cross-section SEM image of PS/ SiN_x structure carried out on p^+ substrate.

The experimental total reflectivity curves are presented in Fig. 5. A refractive index $n = 2.4$ for

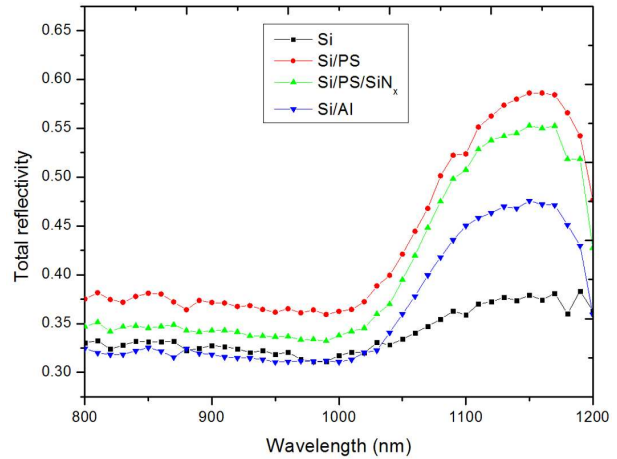


Fig. 5. Experimental total reflectivity spectra for Si/PS and Si/PS/ SiN_x structures compared to Si/Al-BSF contact.

SiN_x layer deposited over to the PS layer (80 to 90 nm thick) achieves 55.5 % of the total reflectivity. The reflectivity improvement is estimated as 8 %, compared to that measured on the surface of Si/BSF-Al contact.

3.3. Internal reflectivity

The values of the measured total reflectivity shown in the previous section are not directly related to the internal reflectivity named R_B , but the external reflectance spectra measured in the long wavelength between 800 and 1200 nm contain information concerning the internal reflectivity.

Optical model of the cell structure presented in Fig. 6 illustrates the total measured reflection (R_T), the internal reflection (R_B) and the internal reflection at the front surface (R_F).

The expression of the extracted internal reflection based on the experimental data of the total reflectivity was detailed in the previous reference [5]. The calculated internal reflection spectra for the structures: Si/PS, Si/PS/ SiN_x and Si/Al are plotted in Fig. 7. The results shown in Fig. 7 prove that the PS and PS/ SiN_x offers an excellent back reflector with a value above 86 %. This improvement is estimated as more than 17 %. Moreover, the calculations showed that the values of R_B remain constant over the range 1100 to 1200 nm. This is due

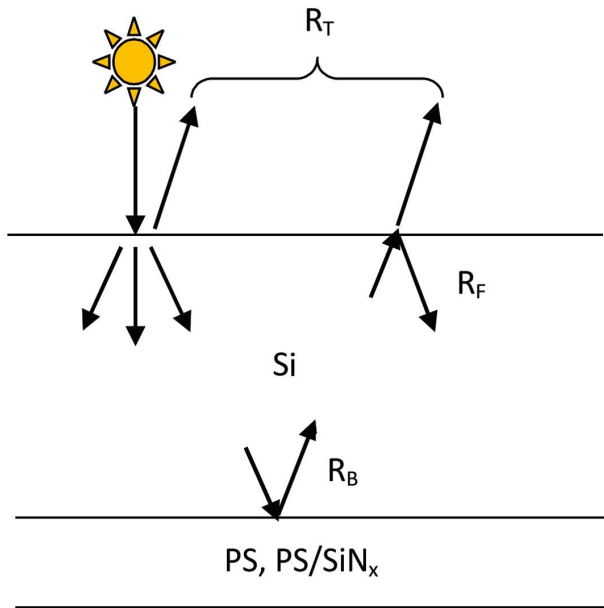


Fig. 6. Optical model of a cell describing the two internal reflections (R_B and R_F) and the total measured reflection (R_T).

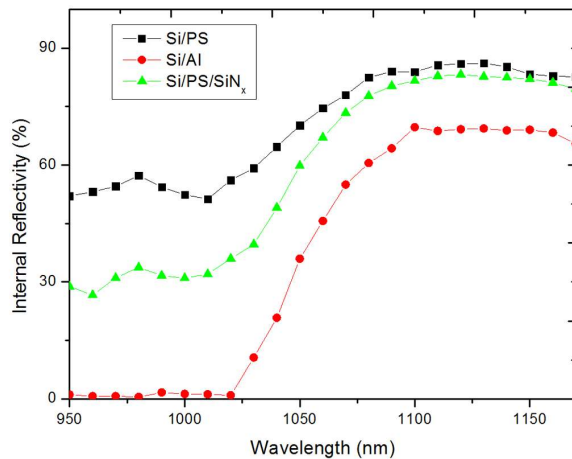


Fig. 7. Internal reflectivity spectra calculated from R_T for Si/PS, Si/PS/SiN_x structures in comparison with the Si/Al reference.

to the refractive indices of the layers which are almost constant in this range. On the other hand, the maximum of the internal reflectivity is obtained at $\lambda = 1130$ nm for the structures. To compare the internal reflectivity for different BRs, the maximum values of R_B at $\lambda = 1130$ nm are presented in Fig. 8a.

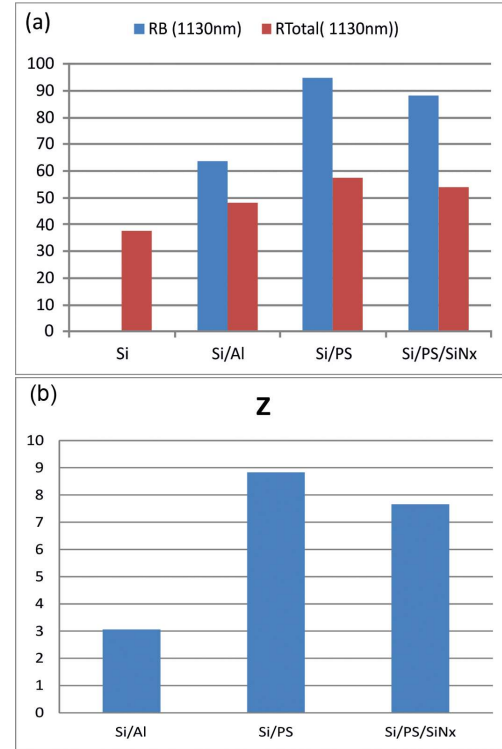


Fig. 8. Total and internal reflectivity at 1130 nm (a), path-length enhancement factor (b), for Si/PS, Si/PS/SiN_x and Si/Al.

To evaluate precisely the quality of the BR for a solar cell, Duerinckx et al. used the path-length enhancement factor (Z), which describes the optical path length for weakly absorbed light. It can be calculated as follows [14]:

$$Z = \frac{1 + R_B}{1 - R_B R_F} \quad (3)$$

where $R_F = 92\%$ for $\lambda = 900 - 1200$ nm is the internal reflectivity at the front. $R_B = 85.84\%$, 82.76% , and 63.66% respectively for Si/PS, Si/PS/SiN_x and Si/Al structures. Values of the optical-path-length enhancement factor (Z) obtained from equation 3 for the back reflector structures are shown in Fig. 8b. The Si/PS (BR) has Z value above eight in the wavelength range of 900 to 1200 nm. We can state that a good optical confinement using the porous silicon layer has been obtained, which can be explained mainly by the difference between the refraction index of the PS (BR) and the substrate ($\Delta n \sim 2$) at $\lambda_0 = 700$ nm.

4. Conclusion

The results of this study show that the internal reflectivity could be significantly enhanced by the use of a single PS layer as a backside reflector for the thin solar cells (less than 150 μm), without changing the current density. 17 % improvement was achieved compared to that extracted from the surface of Si/BSF Al contact. Deposition of the SiN_x LF-PECVD was perfectly carried out on a porous silicon layer. In addition to its passivation properties, the combined PS/ SiN_x layers may also contribute to the improvement of internal reflectivity (14 %). This combination might be the best alternative to the back reflector for silicon solar cells.

Acknowledgements

The authors would like to thank the staff from the NanoLyon Technical Platform for helping in the realization of the structures.

References

- [1] TUCCI M., SERENELLI L., SALZA E., PIROZZI L., DE CESARE G., CAPUTO D., CECCARELLI M., *Mater. Sci. Eng. B-Adv.*, 159 (2009), 48.
- [2] DUERINCKX F., KUZMA-FILIPEK I., NIEUWENHUYSEN K.V., BEAUCARNE G., POORTMANS J., *Prog. Photovoltaic*, 16 (2008), 399.
- [3] BILYALOV R., SOLANKI C.S., POORTMANS J., RICHARD O., BENDER H., KUMMER M., VON KANEL H., *Thin Solid Films*, 170 (2002), 403.
- [4] GHANNAM M.Y., EL-NAGGAR S., RAFAT N., ABOUELSAOOD A.A., *IEEE. T. Electron.*, 46 (1999), 2072.
- [5] CHOULAT P., AGOSTINELLI G., MA F., DUERINCKX F., BEAUCARNE G., 22nd *European Photovoltaic Solar Energy Conference and Exhibition*, Milano, 2007.
- [6] KUSMA-FILIPEK I., DUERINCKX F., NIEUWENHUYSEN K.V., BEAUCARNE G., POORTMANS J., MERTENS R., *Phys. Status Solidi A*, 204 (2007), 1350.
- [7] IVANOV I.I., SKRYSHEVSKY V.A., NYCHYPORUK T., LEMITI M., MAKAROV A.V., KLYUI N.I., TRETYAK O.V., *Renew. Energ.*, 55 (2013), 79.
- [8] GATZ S., HANNEBAUER H., HESSE R., WERNER F., SCHMIDT A., DULLWEBER T., SCHMIDT J., BOTHE K., BRENDL R., *Phys. Status Solidi A*, 4 (2011), 147.
- [9] DUPUIS J., FOURMOND E., NYCHYPORUK O., GIBAJA F., LEMITI M., 23rd *European Photovoltaic Solar Energy Conference*, Valencia, 2008.
- [10] PANEK P., DRABCZYK K., FOCSA A., SLAOU I., *Mater. Sci. Eng B-Adv.*, 165 (2009), 64.
- [11] SLAOU I., PIHAN E., KA I., MBOW N.A., ROQUES S., KOEBEL J.M., *Sol. Energ. Mat. Sol. C.*, 90 (2006), 2087.
- [12] IVANOV I. I., NYCHYPORUK T., SKRYSHEVSKY V.A., LEMITI M., *Semicond. Phys. Quantum Electron. Optoelectron.*, 12 (2009), 406.
- [13] KUZMA-FILIPEK I., DUERINCKX F., NIEUWENHUYSEN K.V., BEAUCARNE G., POORTMANS J., MERTENS R., *Phys. Status Solidi A*, 5 (2006), 1340.
- [14] DUERINCKX F., KUZMA-FILIPEK I., NIEUWENHUYSEN K.V., BEAUCARNE G., POORTMANS J., *IEEE Electr. Device*, 27 (2006), 10.
- [15] GRAU M., NGUYEN N.T., STRABONI A., LEMITI M., *Energy Procedia*, 10 (2011), 8.
- [16] SETZU S., FERRAND P., ROMESTAIN R., *Mater. Sci. Eng B-Adv.*, 69 (2000), 34.
- [17] NYCHYPORUK T., SKRYDHEVSKY V., LEMITI M., 24th *European Photovoltaic Solar Energy Conference*, Hamburg, 2009.
- [18] RAMIZY A., HASSAN Z., OMAR K., AL-DOURI Y., MAHDI M.A., *Appl. Surf. Sci.*, 257 (2011), 6112.
- [19] RAMIZY A., AZIZ W.J., HASSAN Z., OMAR K., IBRAHIM K., *Optik*, 122 (2011), 2075.
- [20] REMACHE L., FOURMOND E., DUPUIS J., MAHDJOUR A., LEMITI M., *Mater. Sci. Eng B-Adv.*, 176 (2011), 45.
- [21] DUPUIS J., LELIČVRE J.F., FOURMOND E., MONGTHE YEN V., NYCHYPORUK O., LE QUANG N., LEMITI M., 24th *European Photovoltaic Solar Energy Conference*, Hamburg, 2009.
- [22] JELLISON G.E., MODINE F.A., *Appl. Phys. Lett.*, 69 (1996), 371.
- [23] ZHAO J., MARTIN., GREEN A., *IEEE. T. Electron. Dev.*, 38 (1991), 1925.
- [24] RIVORY J., *Thin solid films*, 330 (1998), 333.
- [25] MAHDJOUR A., ZIGHED L., *Thin solid films*, 478 (2005), 299.
- [26] PRABAKARAN R., RAGHAVAN G., TRIPURA SUNDARI S., ESAVAMOORTHY R., *Physica E*, 15 (2002), 243.
- [27] PALIK D., *Handbook of Optical Constants of Solids*, Academic Press Handbook Series, Orlando, 1985.
- [28] AROUTIOUNIAN V.M., MARTIROSYAN K.H., SOUKIASSIAN P., *J. Appl. Phys.*, 37 (2002), 25.
- [29] GUPTA A., JAIN V.K., JALWANIA C.R., SINGHAL G.K., ARORA O.P., PURI P.P., SINGH R., PAL M., KUMAR V., *Semicond. Sci. Tech.*, 10 (1995), 698.
- [30] ASTROVA E.V., TOLMACHEV V.A., *Mater. Sci. Eng B-Adv.*, 70 (2000), 142.
- [31] NYCHYPORUK T., *Ph.D. Thesis, INSA-Lyon*, France, 2006.
- [32] REMACHE L., MAHDJOUR A., FOURMOND E., DUPUIS J., LEMITI M., *Phys. Status Solidi C*, (2010), 1.

Received 2015-06-05

Accepted 2015-12-18